frontiers in Materials

ORIGINAL RESEARCH
published: 08 November 2019
doi: 10.3389/fmats.2019.00254

Flame Spray Synthesis of $VOPO_4$ Polymorphs

Gagan Jodhani[1,2], *Fateh Mikaeili*[1] *and Pelagia Irene Gouma*[1,2]*

[1] *Department of Materials Science and Engineering, The Ohio State University, Columbus, OH, United States,* [2] *Department of Materials Science and Engineering, Stonybrook University, Stonybrook, NY, United States*

$VOPO_4$ is a polymorphic compound that exhibits excellent catalytic and electronic properties. Here, formation of different $VOPO_4$ polymorphs using two different organic compounds as precursors is investigated for the first time using flame spray pyrolysis as an alternative method to hydrothermal synthesis of $VOPO_4$, the only method currently known for its synthesis. Ammonium-based salts of vanadium and phosphorous dissolved in aqueous solution were used as precursors for the process. The products from the flame spray pyrolysis process were found to be hollow and amorphous particles in the range of 2–10 μm with shell thicknesses between 200 and 300 nm. Upon calcination and oxidation, the size of spherical particles grew in diameter and crystallization proceeded. However, the surface of calcined particles showed it was composed of smaller grains in the size range of 0.5–1 μm. Finally, the size dependence stability of different polymorphs of $VOPO_4$ is discussed as well as the effect of the different precursors used to stabilize alpha-II and Beta $VOPO_4$ polymorphs.

Keywords: VOPO4, sensors, flame spray pyrolysis, FSP, batteries, li ion batteries, vanadium phosphate

OPEN ACCESS

Edited by:
Xiaogan Li,
Dalian University of Technology (DUT), China

Reviewed by:
Huang Bao Yu,
Dalian University of Technology (DUT), China
Tridib Kumar Sinha,
Gyeongsang National University, South Korea

***Correspondence:**
Pelagia Irene Gouma
gouma.2@osu.edu

Specialty section:
This article was submitted to Functional Ceramics, a section of the journal Frontiers in Materials

Received: *28 June 2019*
Accepted: *25 September 2019*
Published: *08 November 2019*

Citation:
Jodhani G, Mikaeili F and Gouma PI (2019) Flame Spray Synthesis of $VOPO_4$ Polymorphs. Front. Mater. 6:254. doi: 10.3389/fmats.2019.00254

INTRODUCTION

Vanadium phosphates ($VOPO_4$) have gained some noted interest from researchers as functional oxide materials due to their outstanding catalytic and electronic properties. Among their various applications, they have been studied as catalysts for hydrocarbons (Albonetti et al., 1996; Guliants et al., 1996; Coulston et al., 1997; Conte et al., 2006), where the +5 valence state of vanadium is important in the extraction of hydrogen atoms from alkanes (Hutchings et al., 1998). Apart from their applications in catalysis, vanadium phosphates also find applications as electrode materials in lithium-ion batteries (Gaubicher et al., 1999; Kerr et al., 2000; Whittingham et al., 2005) and sodium-ion batteries (He et al., 2016a,b), pseudo capacitors (Wu et al., 2013; Lee et al., 2015), and sensors (Li et al., 2011; Khan et al., 2016). The variety of applications of $VOPO_4$ can be related to the various polymorphs exhibited by the compound.

There are seven reported polymorphs for $VOPO_4$. Among these polymorphs, four exhibit tetragonal structure (α_1, α_2, δ, and ω), two exhibit orthorhombic structure (β and γ) and one monoclinic structure (ε) (Dupré et al., 2004). Among these polymorphs, β-$VOPO_4$ has the lowest energy configuration. However, these polymorphs have been synthesized using various routes; furthermore, due to close relation in the structures of all the polymorphs and their low energy difference, obtaining a single phase is almost impossible (Dupré et al., 2004). The various techniques applied for synthesis of $VOPO_4$ compounds are solvothermal synthesis (Rownaghi et al., 2009; Allen et al., 2011), solid state interactions (Bartley et al., 2001; Sydorchuk et al., 2010), and electrochemical synthesis (Song et al., 2005). However, all these methods either result in big particle size or are commercially unfeasible due to their lengthy processing times.

In this paper, we investigate the Flame Spray Pyrolysis (FSP)-based synthesis of $VOPO_4$ powders. FSP is the process in which a liquid precursor is readily combusted and possesses a high enthalpy reaction, as to sustain the flame. FSP precursors generally consist of high-enthalpy solvents mixed with organometallics (Strobel and Pratsinis, 2007). As such, when the precursor droplets enter the flame zone, the organic solvents are evaporated and can proceed through a particle formation process. However, in cases where the enthalpy of the solution is insufficient, the solute may not sublimate or may partially sublimate and form particles that do not have characteristics of FSP particles (Wang and Huang, 2016). FSP is arguably the more popular flame aerosol technique. This can be attributed to the gas-particle conversion that typically results in finer particles coupled with the homogenous mixing of gaseous elements compared to that of liquid elements (Teoh et al., 2010). Since in an ideal FSP experiment, the particles immediately vaporize, Brownian motion in the gas phase is the dominant factor that determines their final morphology (Ulrich, 1971). The methodology used to produce particles in a laboratory-based FSP setup can be transferred to a foundry for the bulk synthesis of the material. Aeroxide P25 Titania, from Evonik industries, provides evidence for the scalable oxide synthesis via flame aerosol technique. Apart from the commercial aspect, the advantage of flame spray synthesis lies in ease of fabrication, elimination for the use of expensive raw materials, uniform size distribution, and high purity products. Flame-synthesized particles have small particle sizes and high surface area: volume ratios, which is desirable for catalysis and electrochemical processes.

For this study, aqueous solutions with two different organic components as precursors for FSP process are used. The obtained powders are then characterized using XRD, TGA-DTA, SEM, TEM with SAED, and FTIR for their crystallographic phases, morphologies, chemical compositions, and thermal stability.

EXPERIMENTAL METHODS

FSP $VOPO_4$ Using Aqueous Solution With Sucrose

Precursor solution was prepared using ammonium vanadate (1.17 g) and ammonium dihydrogen phosphate (1.15 g). The salts were mixed in 100 ml deionized water, bringing the concentration of the solution to 0.1 M. 1.5 g of sucrose was added to the solution as an organic component. The addition of the organic component was to produce a self-sustaining flame during the FSP process. The solution was stirred at 600 RPM and maintained at 60°C using a heated magnetic stirrer until a homogenous mixture was obtained. The solution was aged for a day and then fed into the FSP system (Tethis NPS 10). For the FSP process, the flame was generated using methane and oxygen, 1.5 slm methane and 3.0 slm oxygen were used, 5 slm oxygen was used as dispersion gas and the solution feed rate was 5 ml. The particles were collected on a glass fiber filter. The powders were calcined at 500°C for 8 h.

FSP $VOPO_4$ Using Aqueous Solution With DMF

Precursor solution was prepared with the same amount of ammonium vanadate and ammonium dihydrogen phosphate. The salts were mixed in 80 ml deionized water. The stirring and heating of the precursor was performed the same as mentioned earlier. A total of 20 ml of DMF, which was used as the organic compound of this solution, was added to make it 0.1 M, which is the same concentration of the other precursor made with sucrose; then, it was fed into the FSP system. The FSP process was done with the same parameters as mentioned in the previous part.

Material Characterization

The powders were characterized using Scanning Electron Microscopy (SEM, LEO 1550), Transmission Electron Microscopy (TEM, JEOL 1400) and selected area electron diffraction was carried out on both as synthesized and calcined samples. Thermogravimetric analysis (TGA, Perkin Elmer Diamond) was conducted on the as-synthesized samples. The particles, both as-synthesized and calcined, were also characterized using XRD (Rigaku Miniflex II) and FTIR (Thermo Scientific Nicolet 6700).

RESULTS

X-Ray Characterization

Figure 1 shows the XRD characterization of FSP-synthesized powders. The as-synthesized particles were relatively amorphous showing significant broad peaks; some extent of crystallinity was obtained. The powders synthesized using a sucrose-based solution, matched with JCPDS 36-0054 for Ammonium Vanadyl Hydrogen phosphate hydrate ($NH_4VOVO_2(HPO_4)_2.1.5H_2O$) and are denoted by the letter A in **Figure 1a**. **Figure 1a** also shows the pattern for powders synthesized using a DMF based solution. The pattern showed a mixed system and matched with JCPDS 36-0054 for Ammonium Vanadyl Hydrogen phosphate hydrate(denoted by A) and JCPDS 34-1247 for tetragonal $VOPO_4$ system(L→ R denoted by α, 200, and 301 planes). The tetragonal $VOPO_4$ system was identified to be α_{II}-$VOPO_4$ based on the lattice parameters (Ling et al., 2014).

Figure 1b shows the XRD characterization of calcined FSP synthesized powders. Both the powders resulted in mixed phases. In the case of calcined powders synthesized with sucrose-based solutions, the peaks from the XRD pattern were found to be orthorhombic β-$VOPO_4$ (JCPDS 71-0859) and tetragonal α_{II}-$VOPO_4$ (JCPDS 34-1247). The peaks for β-$VOPO_4$ are denoted by β(L→ R: 011, 002, 201, 221, 031, 400, and 040 planes) and the peaks for α_{II}-$VOPO_4$ are denoted by α(L→ R: 101, 200, 220, and 132 planes). For calcined powders synthesized with DMF-based solutions, the peaks from XRD pattern were found to be tetragonal δ-$VOPO_4$ (JCPDS 47-0951) and tetragonal α_{II}-$VOPO_4$ (JCPDS 34-1247). The peaks for δ-$VOPO_4$ are denoted by δ(L→ R: 002, 111, 012, 022, 031, 214, and 106 planes) and the peaks for peaks for α_{II}-$VOPO_4$ are denoted by α(L→ R: 101, 111, 200, 220, 112, 301, 311, and 420 planes).

The relative phase content was calculated using peak intensity ratios for all the samples. Quantitative analysis for crystallite size

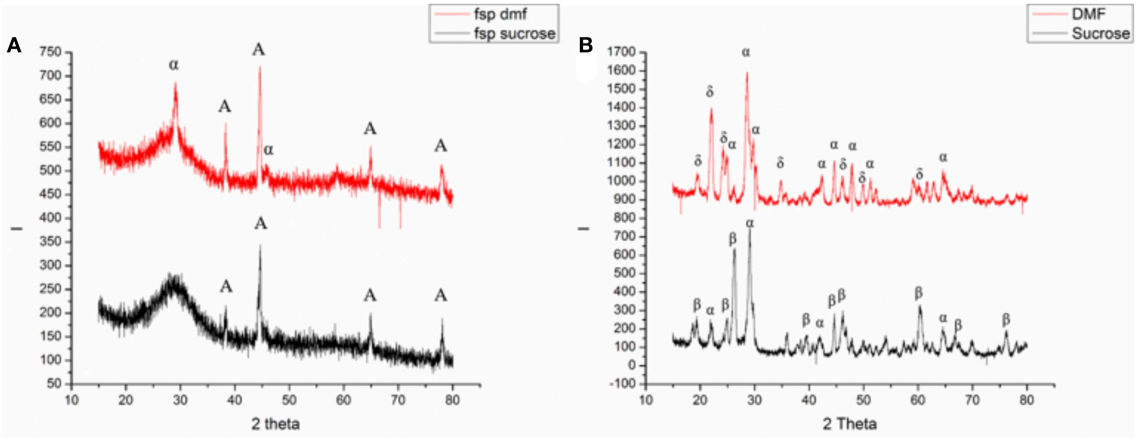

FIGURE 1 | Results of XRD analysis of **(A)** as-synthesized and **(B)** calcined powders [A: Ammonium Vanadyl Hydrogen phosphate hydrate ($NH_4VOVO_2(HPO_4)_2.1.5H_2O$], α: α-$VOPO_4$, β: β- $VOPO_4$, δ: δ- $VOPO_4$).

TABLE 1 | Phase content and crystallite sizes for FSP $VOPO_4$.

Sample	Polymorph	% phase	Crystallite size (nm)
Suc- calcined	β-$VOPO_4$	45.7	26.3
	α_{II}-$VOPO_4$	54.3	24.6
DMF- calcined	δ-$VOPO_4$	42.43	24.3
	α_{II}-$VOPO_4$	57.57	21.7

determination was conducted using Scherrer's formula. **Table 1** lists the phase content and their crystallite sizes.

Thermal Analysis

TGA-DTA was conducted on as-synthesized samples in the range of RT-550°C under oxygen atmosphere. **Figure 2** shows the plot for (a) powders synthesized using sucrose-based solution and (b) powders synthesized using DMF-based solution.

Powders synthesized using sucrose-based solution show a decrease in weight with increase in temperature. The weight loss can be associated with the release of ammonia and water by decomposition of NH_4VOVO_2 $(HPO_4)_2.1.5H_2O$ and formation of $VOPO_4$ structures. The DTA signals show two exothermic changes at 260 and 540°C; these changes can be associated with formation of β-$VOPO_4$ and α_{II}-$VOPO_4$.

Powders synthesized using DMF-based solution also show a decrease in weight with increase in temperature. Similar to the sucrose-based solutions, the weight loss can be associated with the release of ammonia and water by decomposition of $NH_4VOVO_2(HPO_4)_2.1.5H_2O$ and formation of $VOPO_4$ structures. The weight drop stops at 420°C and a slight spike in weight is noticed in the range of 420–550°C. The DTA signals show an exothermic change at 420°C. Since the as-synthesized particles were a mixture of vanadyl hydrogen phosphate hydrate & α_{II}-$VOPO_4$, which resulted in formation α_{II}-$VOPO_4$ and δ-$VOPO_4$, the exothermic reaction at 420°C can be associated with the formation of δ-$VOPO_4$.

Fourier Transform Infrared Spectroscopy

FTIR was conducted on all the samples in the range of 500–4,000 cm^{-1}. The signal received below 500 was erroneous due to significant noise; it was therefore omitted from the results. **Figure 3** shows the FTIR spectra for (a) powders obtained from sucrose-based solution (as-synthesized and calcined) and (b) powders obtained from DMF-based solution (as-synthesized and calcined).

For the as-synthesized particles from the sucrose-based solution, the peaks were obtained at 569, 1,040, 1,424, 1,654, and a broad peak in 3,200 cm^{-1}. The peak at 1,424 cm^{-1} and the broad peak at 3,200 cm^{-1} correspond to the N-H bending vibrations (Socrates, 2004). The peak at 1,654 cm^{-1} indicated presence of water. The strong peak at 1,040 cm^{-1} belongs to P-O (Jiao et al., 1998) vibrations and the peak at 569 cm^{-1} can be associated with V-O-V rotational vibrations (Xue et al., 2010). Upon calcination, the FTIR spectra for the calcined powders revealed peaks at 559, 673, 903, 949, shoulder at 1,080, 1,614, and a broad peak at 3,344 cm^{-1}. The broad peak at 3,344 cm^{-1} and the peak at 1,614 cm^{-1} correspond to N-H bending vibrations (Socrates, 2004) and signify the presence of undecomposed ammonia. The V-O-V rotational vibrations observed at 559 cm^{-1} were observed at 569 cm^{-1} in the calcined sample. Similarly, the peak for P-O vibrations observed at 1,040 cm^{-1} was observed at 1,080 cm^{-1}. New peaks were observed at 673, 903, and 949 cm^{-1}. The peak at 673 can be associated with metaphosphate (Socrates, 2004). The peaks in 903 and 949 cm^{-1} region belong to the V=O vibrations (Anumula et al., 2013). The different peak position signifies a shift in the V=O bonds, the shift can be associated with the presence of two phases.

For the as-synthesized particles from the DMF-based solution, the peaks were obtained at 566, 676, 879, 941, 1,064, 1,426, and 1,644 with a broad peak at 3,200 cm^{-1}. The peak at 1,426 cm^{-1} and the broad peak at 3,200 cm^{-1} correspond to N-H bending vibrations as was the as-synthesized particles from sucrose solution. Similarly, the peak at 1,644 cm^{-1} indicated inclusion of water. The peak at 1,040 cm^{-1} belongs to P-O

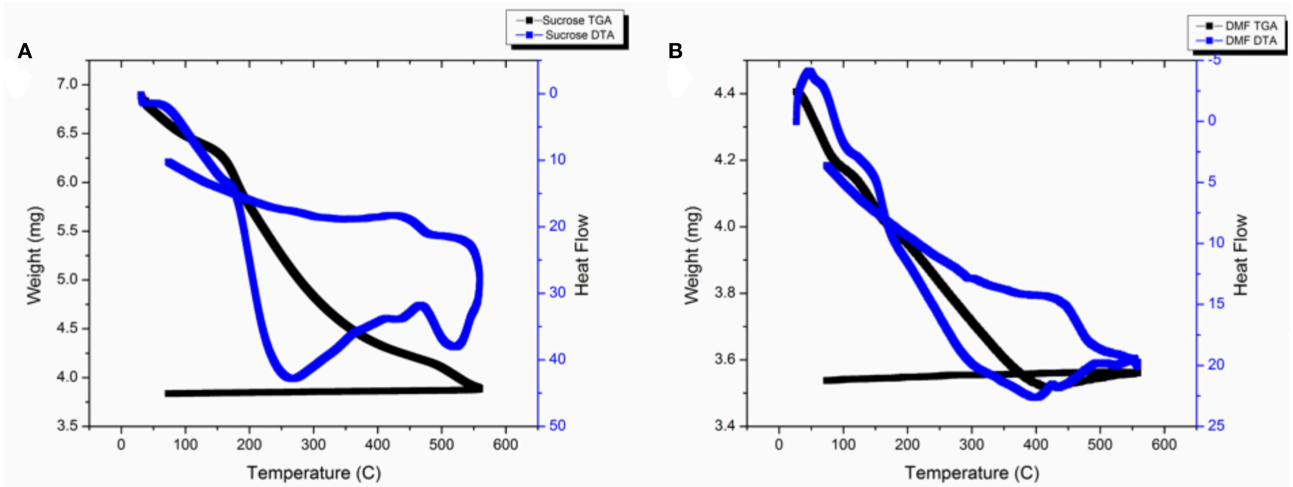

FIGURE 2 | TGA-DTA analysis for **(A)** FSP powders with sucrose **(B)** FSP powders with DMF.

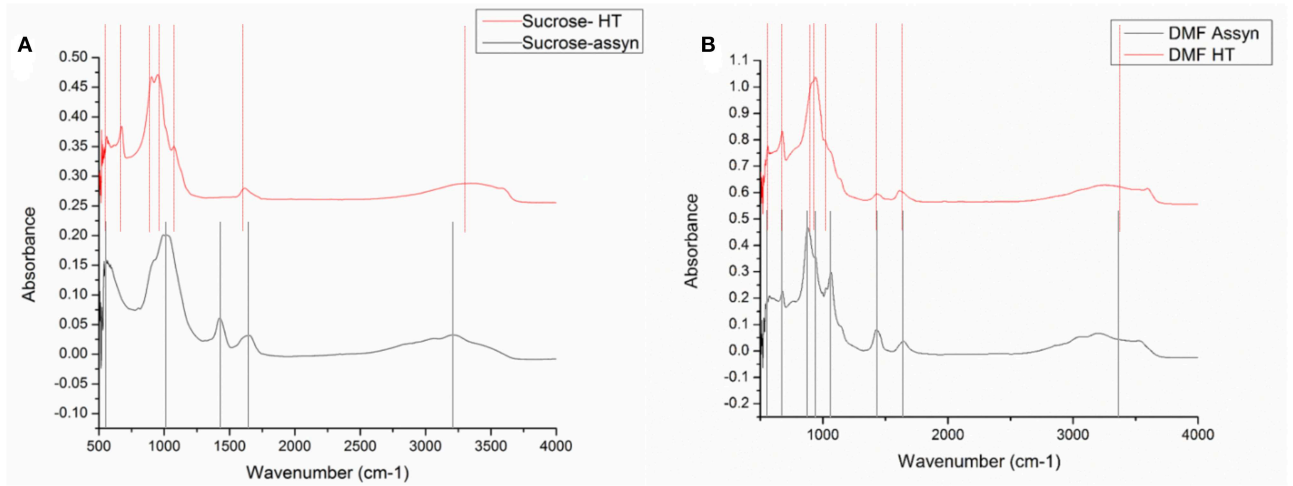

FIGURE 3 | FTIR images for **(A)** as-synthesized and calcined VOPO4 samples synthesized with DMF based precursor **(B)** as- synthesized and calcined VOPO4 samples synthesized with sucrose-based precursor.

vibrations, the peak at 941 belongs to V=O vibrations and the peak at 566 cm^{-1} can be associated with V-O-V rotational vibrations. The peak observed at 873 cm^{-1} corresponds to orthovanadates (Socrates, 2004). Upon calcination, the FTIR spectra for the calcined powders revealed peaks at 560, 674, 939, shoulder at 1,020, 1,428, and 1,612 with a broad peak at 3,254 $cm^{-}1$. The broad peak at 3,254 cm^{-1} and the peak at 1,612 cm^{-1} correspond to N-H bending vibrations (Socrates, 2004) and signify slight presence of undecomposed ammonia. The V-O-V rotational vibrations observed at 566 cm^{-1} were observed at 560 cm^{-1} in the calcined sample. Similarly, the peak for P-O vibrations observed at 1,040 cm^{-1} was observed at 1,020 cm^{-1}, the peak for V=O vibrations observed at 941 cm^{-1} shifted to 939 cm^{-1}, the metaphosphate peak shifted from 676 cm^{-1} to 674 cm^{-1}. A slight shift in peak positions and absence of new peaks indicate that no major change occurred in the structure upon heat treatment.

Scanning Electron Microscopy

The as-synthesized particles and heat-treated samples were characterized by SEM and the particle morphology was analyzed. **Figure 4** shows the SEM images for as-synthesized particles and **Figure 5** compares the SEM images of the heat-treated samples.

As-Synthesized Samples

For the particles synthesized using sucrose-based precursor (**Figures 4a–c**), the particle morphology was in the form of a sphere. Two different sizes of particles were obtained and the large spheres were hollow and in the size range

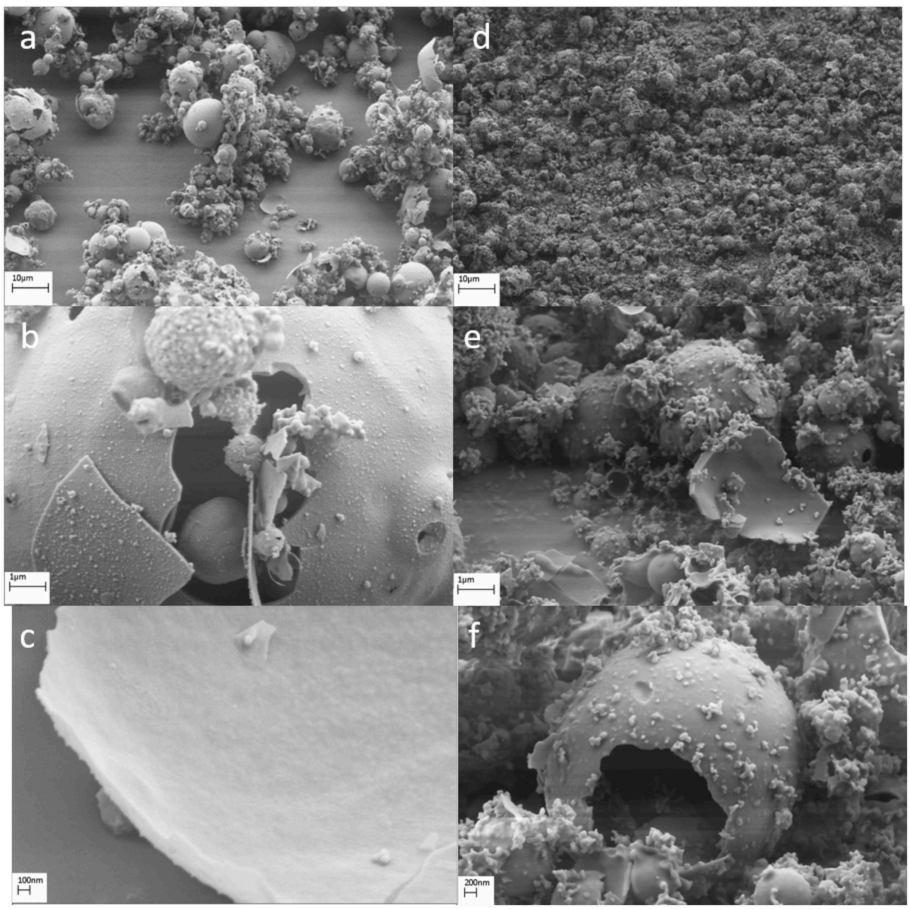

FIGURE 4 | Scanning electron microscopy images for as-synthesized particles from **(a–c)** sucrose-based solutions and **(d–f)** DMF-based solutions.

of 2–10 μm. From high-resolution imaging (**Figure 4c**), the thickness of these was found to be in the range of 100–150 nm. The smaller spheres were solid and in the size range of 200–300 nm. For the particles synthesized using DMF-based precursor (**Figures 4d–f**), the particles were found to be spheres. Similar to the as-synthesized particles from sucrose-based solutions, two different size ranges were noticed. The large spheres were found to be 2–5 μm with a thickness of 50–80 nm. Smaller sized particles were obtained in the range of 50–200 nm.

Calcined Samples

SThe calcined particles were characterized by SEM, and the effect of heat-treatment on particle morphology was analyzed. The particle morphology obtained for calcined particles from sucrose solution (**Figures 5a–c**) was similar to that of as-synthesized samples. The surface of hollow particles was analyzed using a higher resolution and revealed formation of smaller grains on the surface as opposed to an eggshell type of structure for as-synthesized particles. High-resolution imaging (**Figure 5c**) revealed the grain sizes to be in the order of 80–150 nm. The particle morphology obtained for calcined particles from DMF solution (**Figures 5d–f**) was similar to that of as-synthesized samples. However, the grains observed on the surface were found to represent a lamellar structure (**Figure 5f**).

Transmission Electron Microscopy

As-Synthesized Particles

Transmission electron microscopy with selected area electron diffraction was conducted on all samples. The TEM imaging of as-synthesized particles from sucrose-based solution showed thick spherical particles (**Figures 6a,b**). The particles over 1 μm were hollow. SAED pattern did result in any rings (**Figure 6c**), indicating the particles were amorphous, which was already observed in the XRD pattern of the as-synthesized samples. In case of as-synthesized particles from DMF-based solution, solid spheres in the range of 100–200 nm were noticed. No micron-sized particles were found; however, thin walled shell structures were seen indicating disintegration of hollow spheres that were noticed in SEM. SAED pattern on solid spheres resulted in rings that matched with JCPDS 34-1247 α_{II}-$VOPO_4$ (**Figure 6f**; 111 and 220 planes).

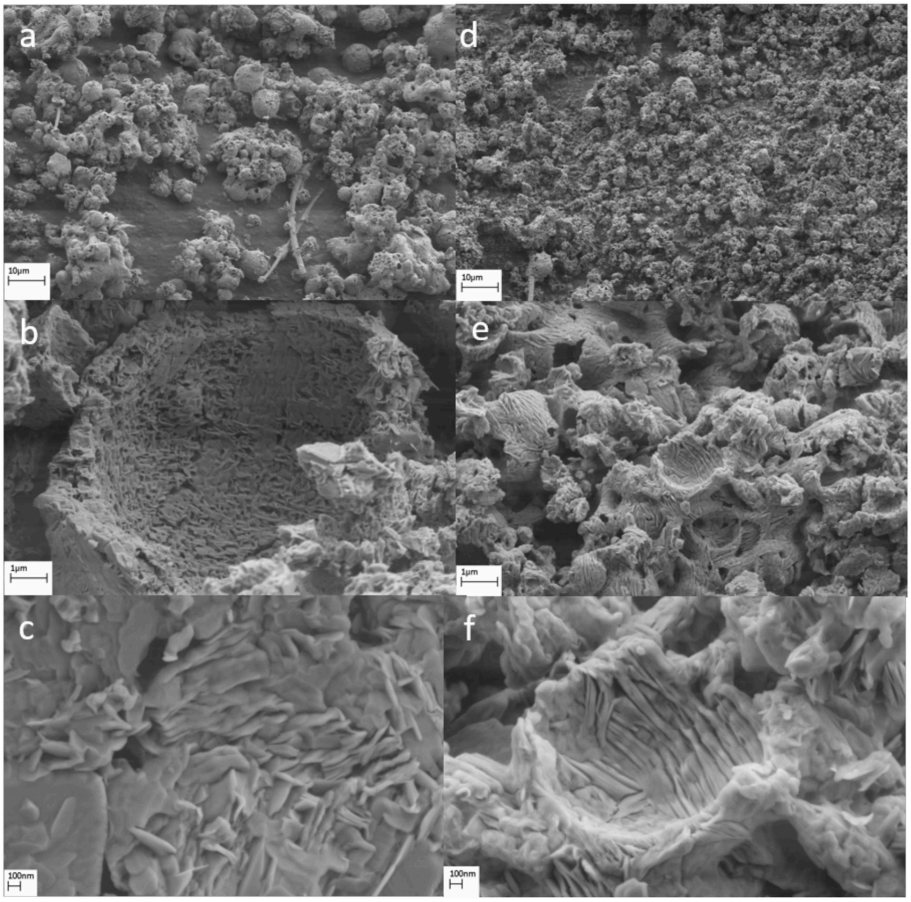

FIGURE 5 | Scanning electron microscopy images for calcined particles from **(a–c)** sucrose based solutions **(d–f)** DMF based solutions.

Calcined Particles

The TEM imaging of calcined particles from sucrose-based solution showed thin spherical disk-like particles (**Figures 7a,b**). The particle sizes for these disks were in the range of 40–300 nm. The SAED pattern on the disks resulted in rings that matched with JCPDS 34-1247 α_{II}-$VOPO_4$ (**Figure 7c**; 200 and 112 planes). No rings were found representing β-$VOPO_4$; however, the imaging showed growth of lathes on the edges of the disks which might be associated with β-$VOPO_4$. In case of calcined particles from DMF-based solution, the morphology was in the form of rectangular nanosheets. The size of these sheets was in the range of 50–500 nm in length. The particle sizes for these disks were in the range of 40–300 nm. SAED pattern on the disks resulted in rings that matched with JCPDS 34-1247 α_{II}-$VOPO_4$ (**Figures 6**, **7f**; 200 and 112 planes).

DISCUSSION

The resultant powders from flame spray pyrolysis (the as-synthesized samples) contained a large amount of $NH_4VOVO_2(HPO_4)_2.1.5H_2O$. The formation of the compound can be attributed to the reaction between ammonium vanadate and ammonium dihydrogen phosphate in aqueous medium. Also, significant difference between the particle sizes could be observed in the as synthesized samples of the two samples with different precursors. As mentioned in the introduction and the experimental sections of the manuscript, the organic components in the FSP precursor are used to produce self-sustaining flame during the FSP process. In the FSP process, the sustainability of the flame is very critical and small changes would lead to drastic changes in particles sizes, morphologies, etc. The particles formed from sucrose-based solutions were in the micron range and hollow, which is usually inconsistent with the results of FSP processing method since the precursor goes through atomization. The formation of such large particles was a result of precursors with low enthalpies coupled with high melting/decomposition points (Teoh et al., 2010). Moreover, due to the usage of an aqueous solution, the temperature of the flame is significantly reduced for complete atomization of particles. However, as it was observed in the SEM results the addition of sucrose helped forming partial submicron sized particles, which is the size range for FSP samples (Purwanto et al., 2011). The formation of organometallics also led to atomization of the precursor and formation of α_{II}-$VOPO_4$.

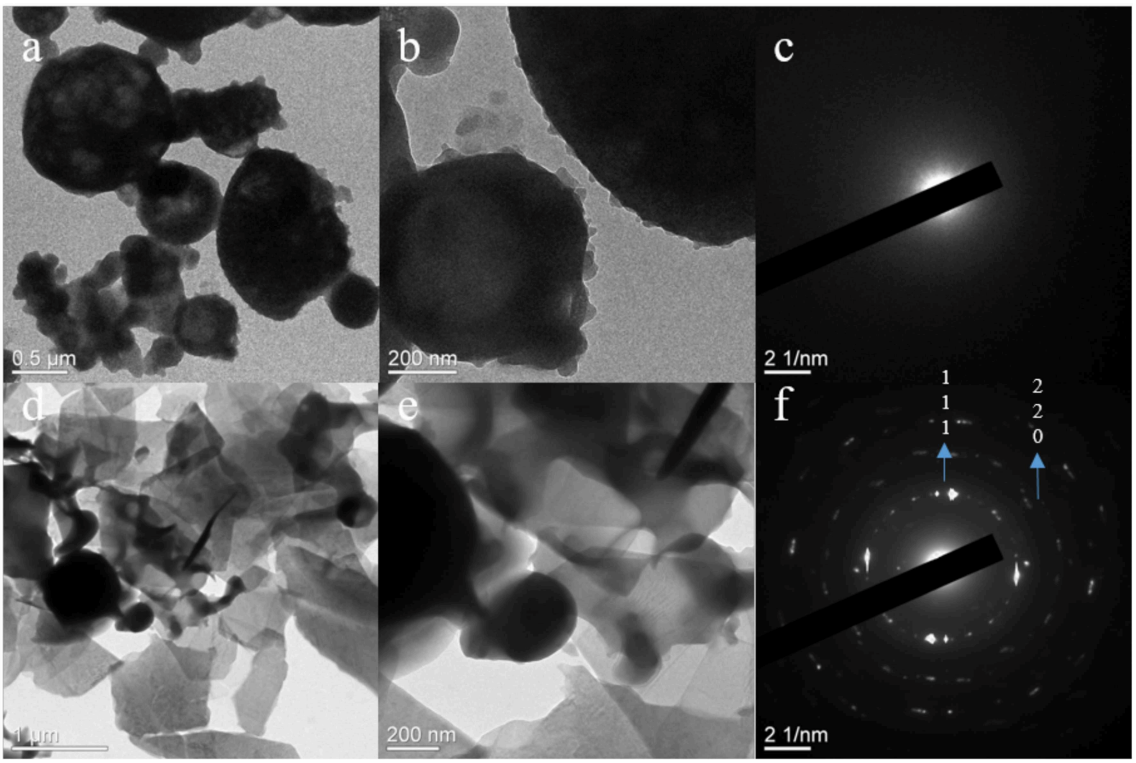

FIGURE 6 | TEM images and corresponding SAED pattern for as-synthesized particles from **(a–c)** sucrose-based solutions and **(d–f)** DMF-based solutions.

Upon calcination of as-synthesized products, the resultant powders were a mixture of α_{II}-$VOPO_4$ & β-$VOPO_4$ and α_{II}-$VOPO_4$ and δ-VOPO4 in the samples synthesized with the sucrose-based precursors and DMF-based precursors, respectively. According to the DFT calculations, the β-$VOPO_4$ is the most stable configuration for $VOPO_4$ (Ling et al., 2014; Sun and Du, 2017). However, based on the same findings, there is only a small difference in energy between $VOPO_4$ polymorphs, which suggests that temperature has little effect on phase transformation in $VOPO_4$. However, it was reported that a slight change in synthesis conditions could lead to the formation of different polymorphs (Dupré et al., 2004). The primary difference in $VOPO_4$ structures occur in the form of V-O bond length, which in turn leads to different crystal structures and polymorphs.

The mixed polymorphs obtained here can be associated with the precursor, where the formation of $NH_4VOVO_2(HPO_4)_2.1.5H_2O$ leads to multiple polymorphs. The precursor salt contains two valence states for VO in the form of $V(IV)O^{2-}$ and $V(V)O_2^-$. The vanadium oxide with +5 valence state exhibits an orthovanadate structure. Based on the results obtained, the orthovanadate structure exhibits similar V-O bond length to α_{II}-$VOPO_4$. Hence, formation of α_{II}-$VOPO_4$ was observed in all the samples. The formation of β and δ polymorphs are a result of the transformation of the +4-valence state VO^{2-} into a +5-valence state in an oxidative atmosphere. The oxidation leads to formation of V-O bond, the length of which determines the formation of either β or δ polymorphs. The oxidation was noticed during the TGA analysis of particles synthesized with the DMF precursor, where a slight increase in weight was observed at 420°C.

In case of powders synthesized using sucrose solution, the VO^{2-} transforms into the most stable state and thereby leads to the formation of β-$VOPO_4$. The synthesis of the δ polymorph has been reported earlier from the thermal oxidation of a +4 valency vanadium hydrogen phosphate compound (Girgsdies et al., 2009). The compound was held at 400°C for 7 days for successful transformation into δ polymorphs. In this study, the lower particle size led to faster transformations.

CONCLUSION

We have successfully demonstrated the formation of different $VOPO_4$ polymorphs with the FSP process. The precursor based on sucrose favors the formation of α_{II}-$VOPO_4$. Furthermore, the reason behind the formation of the secondary phases was addressed due to oxidation of lower valence state vanadium compound in the precursor. Moreover, it was discovered that particle size plays an important role in forming a polymorph upon oxidation of lower valence state compound; smaller particle size favors formation of δ polymorph, whereas large particle sizes tend to form β polymorph. Based on these results, other precursor compounds can be investigated toward formation of other polymorphs for $VOPO_4$.

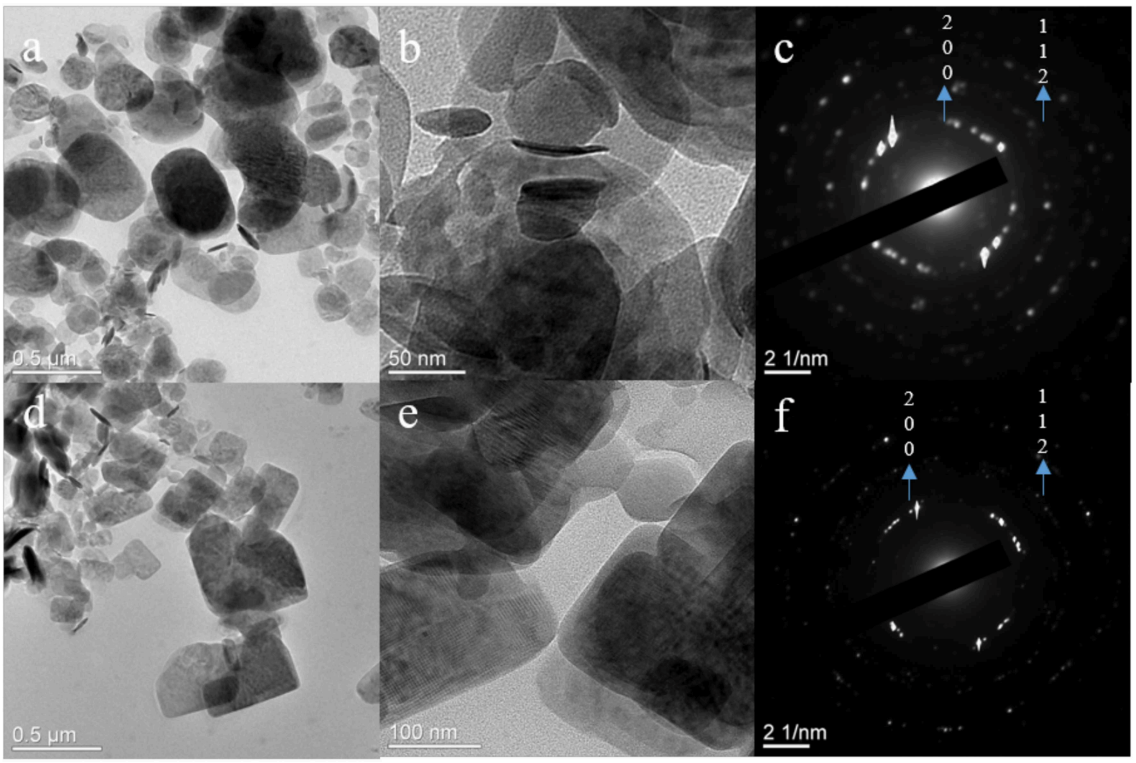

FIGURE 7 | TEM images and corresponding SAED pattern for calcined particles from **(a–c)** sucrose-based solutions and **(d–f)** DMF-based solutions.

DATA AVAILABILITY STATEMENT

All datasets generated for this study are included in the article/supplementary material.

AUTHOR CONTRIBUTIONS

GJ conducted the experiments and wrote the manuscript. FM proofread the manuscript and helped with the analysis of the data. Conceptualization, project administration, and funding acquisition was done by PG.

FUNDING

This project was sponsored by National Science Foundation DMR # 1724455.

REFERENCES

Albonetti, S., Cavani, F., Trifirò, F., and Venturoli, P. (1996). A comparison of the reactivity of "nonequilibrated" and "equilibrated" V-P-O catalysts: structural evolution, surface characterization, and reactivity in the selective oxidation of n-butane and n-pentane. *J. Catal.* 160, 52–64. doi: 10.1006/jcat.1996.0123

Allen, C. J., Jia, Q. Y., Chinnasamy, C. N., Mukerjee, S., and Abraham, K. M. (2011). Synthesis, structure and electrochemistry of lithium vanadium phosphate cathode materials. *J. Electrochem. Soc.* 158, A1250–A1259. doi: 10.1149/2.003112jes

Anumula, R., Nookaraju, M., Selvaraj, K., Reddy, I. A. K., and Narayanan, V. (2013). A novel vanadium n-propylamino phosphate catalyst: synthesis, characterization and applications. *Mater. Res.* 16, 181–189. doi: 10.1590/S1516-14392012005000161

Bartley, J. K., Kiely, C. J., Wells, R. P. K., and Hutchings, G. J. (2001). Vanadium(V) phosphate prepared using solvent-free method. *Catal. Lett.* 72, 99–105. doi: 10.1023/A:1009085127038

Conte, M., Budroni, G., Bartley, J. K., Taylor, S. H., Carley, A. F., Schmidt, A., et al. (2006). Chemically induced fast solid-state transitions of omega-VOPO4 in vanadium phosphate catalysts. *Science* 313, 1270–1273. doi: 10.1126/science.1130493

Coulston, G. W., Bare, S. R., Kung, H., Birkeland, K., Bethke, G. K., Harlow, R., et al. (1997). The kinetic significance of V5+ in n-butane oxidation catalyzed by vanadium phosphates. *Science* 275, 191–193. doi: 10.1126/science.275.5297.191

Dupré, N., Wallez, G., Gaubicher, J., and Quarton, M. (2004). Phase transition induced by lithium insertion in αI- and αII-VOPO4. *J. Solid State Chem.* 177, 2896–2902. doi: 10.1016/j.jssc.2004.04.006

Gaubicher, J., Le Mercier, T., Chabre, Y., Angenault, J., and Quarton, M. (1999). Li/beta-VOPO4: a new 4 V system for lithium batteries. *J. Electrochem. Soc.* 146, 4375–4379.

Girgsdies, F., Schneider, M., Brückner, A., Ressler, T., and Schlögl, R. (2009). The crystal structure of δ-VOPO4 and its relationship to ω-VOPO4. *Solid State Sci.* 11, 1258–1264. doi: 10.1016/j.solidstatesciences.2009.03.017

Guliants, V. V., Benziger, J. B., Sundaresan, S., Wachs, I. E., Jehng, J.-M., Roberts, J. E., et al. (1996). The effect of the phase composition of model VPO catalysts for partial oxidation of n-butane. *Catal. Today* 28, 275–295. doi: 10.1016/S0920-5861(96)00043-0

He, G., Huq, A., Kan, W. H., and Manthiram, A. (2016a). beta-NaVOPO4 obtained by a low-temperature synthesis process: a new 3.3 V cathode for sodium-ion batteries. *Chem. Mater.* 28, 1503–1512. doi: 10.1021/acs.chemmater.5b04992

He, G., Kan, W. H., and Manthiram, A. (2016b). A 3.4 V layered VOPO4 cathode for Na-Ion batteries. *Chem. Mater.* 28, 682–688. doi: 10.1021/acs.chemmater.5b04605

Hutchings, G. J., Kiely, C. J., Sananes-Schulz, M. T., Burrows, A., and Volta, J. C. (1998). Comments on the nature of the active site of vanadium phosphate catalysts for butane oxidation. *Catal. Today* 40, 273–286. doi: 10.1016/S0920-5861(98)00015-7

Jiao, X., Chen, D., Pang, W., Xu, R., and Yue, Y. (1998). Solvothermal synthesis and characterization of silica-pillared titanium phosphate. *J. Mater. Chem.* 8, 2831–2834. doi: 10.1039/a802838i

Kerr, T. A., Gaubicher, J., and Nazar, L. F. (2000). Highly reversible Li insertion at 4 V in epsilon-VOPO4/alpha-LiVOPO4 cathodes. *Electrochem. Solid State Lett.* 3, 460–462. doi: 10.1149/1.1391179

Khan, A., Khan, A. A. P., Rahman, M. M., and Asiri, A. M. (2016). High performance polyaniline/vanadyl phosphate (PANI-VOPO4) nano composite sheets prepared by exfoliation/intercalation method for sensing applications. *Eur. Poly. J.* 75, 388–398. doi: 10.1016/j.eurpolymj.2016.01.003

Lee, K. H., Lee, Y. W., Lee, S. W., Ha, J. S., Lee, S. S., and Son, J. G. (2015). Ice-templated Self-assembly of VOPO4-graphene nanocomposites for vertically porous 3D supercapacitor electrodes. *Sci. Rep.* 5:13696. doi: 10.1038/srep13696

Li, G. C., Li, Y. M., Li, Y., Peng, H. R., and Chen, K. Z. (2011). Polyaniline nanorings and flat hollow capsules synthesized by in situ sacrificial oxidative templates. *Macromolecules* 44, 9319–9323. doi: 10.1021/ma2014854

Ling, C., Zhang, R., and Mizuno, F. (2014). Phase stability and its impact on the electrochemical performance of VOPO4 and LiVOPO4. *J. Mater. Chem. A* 2, 12330–12339. doi: 10.1039/C4TA01708K

Purwanto, A., Wang, W. N., and Okuyama, K. (2011). "Flame spray pyrolysis," in *Handbook of Atomization and Sprays*, ed N. Ashgriz (Boston, MA: Springer)

Rownaghi, A., Taufiq-Yap, Y. H., and Rezaei, F. (2009). Solvothermal synthesis of vanadium phosphate catalysts for n-butane oxidation. *Chem. Eng. J.* 155, 514–522. doi: 10.1016/j.cej.2009.07.055

Socrates, G. (2004). *Infrared and Raman Characteristic Group Frequencies: Tables and Charts*. John Wiley & Sons.

Song, Y., Zavalij, P. Y., and Whittingham, M. S. (2005). ε-VOPO4: electrochemical synthesis and enhanced cathode behavior. *J. Electrochem. Soc.* 152, A721–A728. doi: 10.1149/1.1862265

Strobel, R., and Pratsinis, S. E. (2007). Flame aerosol synthesis of smart nanostructured materials. *J. Mater. Chem.* 17, 4743–4756. doi: 10.1039/b711652g

Sun, W., and Du, J. (2017). Structural stability, electronic and thermodynamic properties of VOPO4 polymorphs from DFT+U calculations. *Comput. Mater. Sci.* 126, 326–335. doi: 10.1016/j.commatsci.2016.09.046

Sydorchuk, V., Khalameida, S., Zazhigalov, V., Skubiszewska-Zieba, J., and Leboda, R. (2010). Solid-state interactions of vanadium and phosphorus oxides in the closed systems. *J. Thermal Anal. Calorimetry* 100, 11–17. doi: 10.1007/s10973-010-0696-x

Teoh, W. Y., Amal, R., and Mädler, L. (2010). Flame spray pyrolysis: an enabling technology for nanoparticles design and fabrication. *Nanoscale* 2, 1324–1347. doi: 10.1039/c0nr00017e

Ulrich, G. D. (1971). Theory of particle formation and growth in oxide synthesis flames. *Combust. Sci. Technol.* 4, 47–57. doi: 10.1080/00102207108952471

Wang, S. H., and Huang, Y. (2016). Flame aerosol synthesis of WO3/CeO2 from aqueous solution: two distinct pathways and structure design. *Chem. Eng. Sci.* 152, 436–442. doi: 10.1016/j.ces.2016.06.045

Whittingham, M. S., Song, Y. N., Lutta, S., Zavalij, P. Y., and Chernova, N. A. (2005). Some transition metal (oxy)phosphates and vanadium oxides for lithium batteries. *J. Mater. Chem.* 15, 3362–3379. doi: 10.1039/b501961c

Wu, C., Lu, X., Peng, L., Xu, K., Peng, X., Huang, J., et al. (2013). Two-dimensional vanadyl phosphate ultrathin nanosheets for high energy density and flexible pseudocapacitors. *Nat. Commun.* 4:2431. doi: 10.1038/ncomms3431

Xue, M., Chen, H., Zhang, H., Auroux, A., and Shen, J. (2010). Preparation and characterization of V-Ag-O catalysts for the selective oxidation of toluene. *Appl. Catal. A Gen.* 379, 7–14. doi: 10.1016/j.apcata.2010.02.023

Conflict of Interest: The authors declare that the research was conducted in the absence of any commercial or financial relationships that could be construed as a potential conflict of interest.